Vol. 13, No. 37, Winter 2024, pages 11-19

Journal of Analytical and Numerical Methods in Mining Engineering

Journal home page: http://anm.yazd.ac.ir/

Research article

Modifying Drucker-Prager Criterion for Elastoplastic Porous Rocks Using a Numerical Integration Algorithm

Manouchehr Sanei[1*]

1- Dept. of Mining and Metallurgy Engineering, Yazd University, Yazd, Iran.

*Corresponding author: E-mail: *m.sanei@yazd.ac.ir*

(Received: *September 2023*, Accepted: *November 2023)*

DOI: 10.22034/ANM.2023.20576.1608

Keywords

Elastoplastic
Drucker-Prager
Integration algorithm
Return mapping
Porous Rock

Abstract

In the topics related to rock mechanics and geotechnics, elastoplastic criteria are of special importance. This importance makes their numerical implementation necessary. Although most of the existing software in the field of rock mechanics and geotechnics have elastoplastic criteria, the lack of access to their coding core makes it practically impossible for researchers to develop them. Therefore, considering the importance of elastoplastic criteria and the complexity of their implementation, in this study, a suitable scheme was presented to improve the elastoplastic numerical integration algorithm of Darker-Prager criteria. The developed algorithm includes two steps of elastic trial and plastic return-mapping algorithm. In the proposed model, if the elastic trial step is in the elastic domain or on the yield surface, the answer of elasticity is approved. Otherwise, if the trial stress can not confirm the desired conditions in the first step, it is executed by the plastic return-mapping algorithm. This process has been done comprehensively and separately for Drucker-Prager's cone and apex to be able to express the elastoplastic behavior of the material optimally. The presented model was analyzed for the porous rock sample and its validation was confirmed by comparing the numerical results with the laboratory data.

1. INTRODUCTION

The behavior of materials under extreme loading conditions is usually described by plasticity models. The plastic behavior of a wide range of geotechnical and rock mechanics materials such as rock, soil, concrete, and porous media is dependent on hydrostatic stress. In 1952, an approximation of the Mohr-Coulomb criterion was proposed by Drucker and Prager as a modification of the von Mises criterion. The Drucker-Prager criterion is widely used to model the behavior of geomaterials to consider the influence of the hydrostatic stress component on the material [1]. In addition, the yield surface of Drucker-Prager is represented with a cone in the principal stress space.

In solving engineering problems that involve plastic deformation of materials, it is generally essential to express the finite element method along with the use of plasticity theories. In nonlinear finite element analysis, one of the basic steps is to update the stress at each Gaussian point for incremental strains. The stresses are updated by integrating the local constitutive equations. This process is carried out by a convenient method or an approximate scheme that requires a lot of calculations, even if this process is expressed for simple plasticity theories [2]. This process is usually presented by a numerical integration algorithm of elastoplastic constitutive equations [3].

The Drucker-Prager criterion is often used to simulate the behavior of geomaterials. While this criterion is one of the most common constitutive equations, it still creates extensive challenges and complexities for implementation.

The implementation of the Drucker-Prager model in the finite element method demands the use of numerical integration algorithms for presenting the incremental evolution of stresses [4]. Within the last decade, various integration algorithms have been proposed and categorized for the implementation of the Drucker-Prager model. Based on this, Loret and Preust [5] presented an exact numerical solution for the Drucker-Prager model. The presented method was a bit time-consuming. Genna and Pandolfi [6] presented a two-step integration scheme for the rate-of-plasticity equations of the Drucker-Prager model. Kobayashi et al. [7], Kan et al. [8], and Coombs et al. [9] extended the backward Euler integration for the constitutive equations. Liu [10] investigated internal symmetries for the Drucker-Prager's material model. Rezaiee-Pajand and Nasirai [3] expressed two stress-updating schemes in a semi-implicit method for the Drucker-Prager plasticity with no hardening. Rezaiee-Pajand et al. [1] presented accurate and approximate integrations of Drucker-Prager plasticity with linear hardening.

Previous studies show that the numerical integration algorithm for elastoplastic constitutive models has certain complications. Algorithm development is unique for each constitutive model.

In some sources, this numerical approach is based on two main steps [4]: the elastic trial step and a subsequent return-mapping scheme. The convergence rate of the iterative method for solving nonlinear elastoplastic equations generally depends on the choice of variables [11].

Due to the importance of the Darker-Prager criterion and the lack of access to the programming coding core of the software that has the mentioned criterion, the necessity of implementing this model is inevitable. On the other hand, the complexities of implementing this model require the development of the most appropriate elastoplastic integration algorithm, which, in addition to convergence, has a high convergence speed .

Therefore, in this study, considering the importance of the subject, a suitable scheme for the elastoplastic integration algorithm of the Drucker-Prager criterion is proposed. The proposed integration algorithm includes two steps of elastic trial step and a subsequent return-mapping scheme. In the proposed model for the Drucker-Prager criterion, if the elastic trial state is in the elastic domain or on the yield surface, the answer of elasticity is accepted. Otherwise, if the trial stress cannot confirm the desired conditions in the first step, it will be presented again by the stress return-mapping algorithm. This process is carried out comprehensively and separately for Drucker-Prager's cone and apex in order to be able to properly show the elastoplastic behavior of the material during loading. The proposed approach for the Drucker-Prager criterion is confirmed and validated by comparing the numerical and experimental results.

2. ELASTOPLASTIC CONSTITUTIVE MODEL

Any nonlinear elastoplastic constitutive model can be described by elastoplastic theory. When a material undergoes irreversible changes under the influence of specific loading conditions. The total strain tensor ε is divided into two components of elasticity and plasticity as follows [12-15]:

$$\varepsilon = \varepsilon_e + \varepsilon_p \tag{1}$$

where ε_e is the elastic strain and ε_p is the plastic strain. During loading, the elastic component is reversible and the plastic component represents permanent deformation and is related to the history of irreversible deformations [16-18]. In these problems, when a displacement u is determined, the relationship between strain and displacement under the infinitesimal strain theory is defined as follows [19-21]:

$$\varepsilon = \frac{1}{2}(\nabla u + \nabla^T u) \tag{2}$$

2.1. Elastoplastic Deformation

Elastoplastic deformation is mathematically described using four basic principles as follows [20]:

Elastic law. It can be defined by using the linear stress-strain relationship as follows [22]:

$$div(\sigma - \sigma^o) = 0 \tag{3}$$

where σ^o and σ are the initial and current Cauchy total stress [MPa], respectively. The total stress σ is obatined by linear stress-strain relationship, as follows [22]:

$$\sigma - \sigma^o = 2\mu(\varepsilon_e - \varepsilon_e^o) + \lambda\, tr(\varepsilon_e - \varepsilon_e^o)I \tag{4}$$

where ε_e^o and ε_e are the initial and current elastic strain. The parameters μ and λ are the elastic Lamé constants [MPa].

Yield criterion. It states the elastic and plastic part through a plasticity yield function $\Phi =$

$\Phi(\sigma, A)$, where $A = \overline{\rho}\partial F^p/\partial\chi$ is the hardening thermodynamic force, F^p is the plastic part of Helmholtz free energy F, and χ is the hardening variable [23].

Flow rule. It describes the plasticity process $\dot{\varepsilon} = \gamma N$, in which $N(\sigma, A) = \partial\Psi/\partial\sigma$ is the flow direction and $\dot{\gamma}$ is the plastic multiplier. The flow rule is named associative if the plastic potential function Ψ equals to yield function Φ, namely $\Psi = \Phi$ [24-26].

Hardening law. It shows how the internal damage variable $\dot{\chi} = \dot{\gamma}H$ evolves, in which, $H(\sigma, A) = -\partial\Psi/\partial A$ is the hardening modulus.

2.2. Drucker-Prager Criterion

The Drucker-Prager criterion has been proposed by Drucker and Prager [27] as a smooth approximation to the Mohr–Coulomb criterion. This criterion consists of a modification of the von Mises criterion in which an extra part is involved to present pressure-sensitivity. The Drucker-Prager model is suitable for materials such as soil, rock, concrete, and porous media. The Drucker-Prager model consists of three key principles, namely: (a) elastic law, (b) yield function, and (c) flow law.

Drucker-Prager's elastic law:

The elastic law of the Drucker-Prager model is defined using the linear elastic stress-strain relationship that was expressed in Eq. (4).

Drucker-Prager's yield function:

The Drucker–Prager yield function expresses that plastic yielding starts when the J_2 invariant of the deviatoric stress and the hydrostatic stress, p, arrive at a critical combination. The begin of plastic yielding happens when the equation is contented, as [26]:

$$\sqrt{J_2(s)} + \eta\, p = \bar{c} \tag{5}$$

where η and $\bar{c}$ are material parameters. Appointed in the principal stress space, the yield locus of this criterion is a circular cone which axis is the hydrostatic line. For $\eta = 0$, the von Mises cylinder is retrieved. The Drucker–Prager cone is illustrated in Fig. 1.

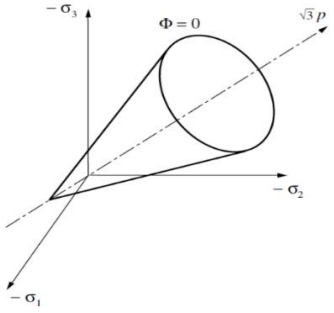

Fig. 1 . The Drucker–Prager yield surface in principal stress space [4].

To be able to approximate the Drucker–Prager yield surface, it is adequate to express the Drucker–Prager yield function as [27]:

$$\Phi(\sigma, c) = \sqrt{J_2\big(s(\sigma)\big)} + \eta\, p(\sigma) - \xi c \tag{6}$$

where c is the cohesion and the parameters η and ξ are selected according to the needed approximation to the Mohr–Coulomb criterion.

Two of the most general approximations applied are computed by creating the yield surfaces of the Drucker–Prager and Mohr–Coulomb criteria coincided with either at the outer or inner edges of the Mohr–Coulomb surface. Coinciding with the outer edges can be computed when [4]:

$$\eta = \frac{6\sin\emptyset}{\sqrt{3}(3 - \sin\emptyset)} \qquad \xi = \frac{6\cos\emptyset}{\sqrt{3}(3 - \sin\emptyset)} \tag{7}$$

whereas, coinciding with the inner edges can be presented by the choice [4]:

$$\eta = \frac{6\,sin\,\emptyset}{\sqrt{3}(3 + sin\,\emptyset)} \qquad \xi = \frac{6\,cos\,\emptyset}{\sqrt{3}(3 + sin\,\emptyset)} \tag{8}$$

where $\emptyset$ is internal friction angle. The outer and inner cones are introduced, respectively, as the compression cone and the extension cone.

Another Drucker–Prager approximation for the Mohr–Coulomb criterion is using collapse loads under plane strain conditions, which the constants η and ξ are expressed as follows [28]:

$$\eta = \frac{3\tan\emptyset}{\sqrt{9 + 12\tan^2\emptyset}} \qquad \xi = \frac{3}{\sqrt{9 + 12\tan^2\emptyset}} \tag{9}$$

In the Eq. (6), J_2 can be expressed as:

$$J_2 = \frac{1}{2}s{:}\,s \tag{10}$$

where,

$$s = \sigma - p(\sigma)I \tag{11}$$

where $p = \frac{1}{3}tr[\sigma]$ is the hydrostatic pressure.

Drucker-Prager's flow rule:

The associative flow rule, which is the yield function Φ is the same as flow potential Ψ, is adopted to present the Drucker-Prager criterion.

The flow potential of associative Drucker-Prager is [4]:

$$\Psi(\sigma, \mathrm{c}) = \sqrt{\mathrm{J}_2\big(s(\sigma)\big)} + \eta\, p(\sigma) - \xi \mathrm{c} \tag{12}$$

The flow potential of non-associative Drucker-Prager is [4]:

$$\Psi(\sigma, \mathrm{c}) = \sqrt{\mathrm{J}_2\big(s(\sigma)\big)} + \bar{\eta}\, p(\sigma) \tag{13}$$

where the constant $\bar{\eta}$ is dependent on the dilatancy angle. The flow rule of Drucker-Prager can be defined as [2]:

$$\dot{\varepsilon}_p = \dot{\gamma}\, N \tag{14}$$

where, on the smooth portion of the yield surface, the flow vector is presented as [2]:

$$N = \frac{\partial \Psi}{\partial \sigma} \tag{15}$$

3. NUMERICAL INTEGRATION ALGORITHM FOR THE ELASTOPLASTIC MODEL

The numerical integration is divided into two main stages: the elastic trial step and the plastic corrector step. If the elastic trial step is in the elastic domain or on the yield surface, the solution is accepted. Otherwise, if the trial stress in the first step fails to confirm the acceptable plastic condition, it is projected by the return mapping algorithm onto the yield surface [20].

The incremental constitutive model is obtained by providing the elastic strain $\boldsymbol{\varepsilon}_e^{n-1}$, the plastic strain $\boldsymbol{\varepsilon}_p^{n-1}$, and the hardening variable χ^{n-1} at a time step t^{n-1}, as well as considering an incremental strain tensor $\Delta\boldsymbol{\varepsilon}$ for the time interval $[t^{n-1}, t^n]$ to obtain subsequent equations in a time-step t^n, as [20]:

$$\begin{aligned} \varepsilon_e^n &= \varepsilon_e^{n-1} + \Delta\varepsilon - \Delta\gamma N(\sigma^n, A^n) \\ \chi^n &= \chi^{n-1} + \Delta\gamma H(\sigma^n, A^n) \end{aligned} \tag{16}$$

for the unknowns $\boldsymbol{\varepsilon}_e^n$,, χ^n and the incremental of plastic multiplier $\Delta\gamma$, it has following restrictions [20]:

$$\Delta\gamma \geq 0, \Phi(\sigma^n, A^n) \leq 0, \Delta\gamma\Phi(\sigma^n, A^n) = 0 \tag{17}$$

The elastoplastic problem is solved in two steps. Firstly, an elastic answer is calculated, in which, $\Delta\gamma = 0$ and the elastic trial stress is $\boldsymbol{\varepsilon}_{e_{trial}}^n = \boldsymbol{\varepsilon}_e^{n-1} + \Delta\boldsymbol{\varepsilon}$, as well as the hardening variable is $\chi_{trial}^n = \chi^{n-1}$. Next, σ_{trial}^n and $\Phi(\boldsymbol{\sigma}_{trial}^n, \boldsymbol{A}_{trial}^n)$ are obtained based on $\boldsymbol{\varepsilon}_{e_{trial}}^n$. If $\Phi(\sigma_{trial}^n, A_{trial}^n) \leq 0$, the elastic answer is valid, then the elastoplastic parameters are updated using the trial values $(\cdot)^n := (\cdot)_{trial}^n$. Otherwise, the return-mapping algorithm is required to update such nonlinear relationships as [20]:

$$\begin{aligned} &\varepsilon_e^n = \varepsilon_{e_{trx}}^n - \Delta\gamma N(\sigma^n, A^n) \\ &\chi^n = \chi_{trial}^n + \Delta\gamma H(\sigma^n, A^n) \\ &\Delta\gamma > 0, \Phi(\sigma^n, A^n) = 0 \end{aligned} \tag{18}$$

When the elastic strain $\boldsymbol{\varepsilon}_e^n$ is calculated, thus the plastic strain is updated in a time step t^n as follows [20, 29, 30]:

$$\varepsilon_p^n = \varepsilon_p^{n-1} + \Delta\varepsilon - \Delta\varepsilon_e \tag{19}$$

3. 1. Numerical Integration Algorithm For The Drucker-Prager Model

The integration algorithm for the Drucker-Prager model can be presented by considering the common return-mapping update formula for the stress tensor as follows [2, 4]:

$$\sigma^n = \sigma_{tiral}^n - \Delta\gamma D_e : N^n \tag{20}$$

where $-\Delta\gamma D_e N^n$ is the return vector. As a consequence of the symmetry about the pressure axis, whenever the above equation is used, the return vector is parallel to the plane that includes $\boldsymbol{\sigma}_{tiral}^n$ and hydrostatic axis. To be able to implement the Drucker-Prager criterion, the return-mapping algorithm is presented by two separately part including cone and apex.

Return-mapping of the cone

On the cone, the flow vector is expressed by Eq. (15). The increment of plastic strain is [4]:

$$\dot{\varepsilon}_p = \dot{\gamma} N^n = \Delta\gamma \left(\frac{1}{2\sqrt{J_2(s)}} s_n + \frac{\bar{\eta}}{3} I \right) \tag{21}$$

The stress update is [4]:

$$\begin{aligned} \sigma^n &= \sigma_{tiral}^n - \Delta\gamma [2G(N^d)^n \\ &\qquad + K(N^v)^n] \\ &= \sigma_{tiral}^n - \Delta\gamma \left[\frac{G}{\sqrt{J_2(s)}} s_n + \frac{K\,\bar{\eta}}{3} I \right] \end{aligned} \tag{22}$$

The simplification of the above equation is [4]:

$$\sigma^n = \sigma_{tiral}^n - \Delta\gamma \left[\frac{G}{\sqrt{J_2(s)}} s_n^{trial} + \frac{K\,\bar{\eta}}{3} I \right] \tag{23}$$

The deviatoric and hydrostatic components are [4]:

$$s^n = \left(1 - \frac{G\dot{\gamma}}{\sqrt{J_2(s_n^{trial})}}\right) s_{tiral}^n \tag{24}$$

$$p^n = p_{tiral}^n - K\,\bar{\eta}\Delta\gamma$$

The consistency condition for associative function is [4]:

$$\Phi_n = \sqrt{J_2(s^n)} + \eta\, p^n - \xi c(\boldsymbol{\varepsilon}_p^n) = 0 \tag{25}$$

The consistency condition for non-associative function is [4]:

$$\Phi_n = \sqrt{J_2(s^n)} + \bar{\eta}\, p^n = 0 \tag{26}$$

where the update plastic strain is [4]:

$$\varepsilon_p^n = \varepsilon_p^{n-1} + \Delta\varepsilon_p \tag{27}$$

with

$$\Delta\boldsymbol{\varepsilon}_p = \xi\Delta\gamma \tag{28}$$

By substituting the Eqs. (27) and (24) into the consistency condition for $\Delta\gamma$, the following equation is obtained [4]:

$$\Phi_n(\Delta\gamma) = \sqrt{J_2(s_n^{trial})} - G\Delta\gamma + \eta\,(p_{tiral}^n - K\,\bar{\eta}\Delta\gamma) - \xi c(\boldsymbol{\varepsilon}_p^{n-1} + \xi\Delta\gamma) = 0 \tag{29}$$

After solving the Eq. (29), the stress is updated. The return-mapping on the cone is shown schematically in Fig. 2(a).

Return-mapping of the apex

At the apex, the return vector should be in the complementary cone illustrated schematically in Fig. 2(b). In this situation, the consistency condition in Eq. (25) is as follows [4]:

$$c(\boldsymbol{\varepsilon}_p^{n-1} + \Delta\boldsymbol{\varepsilon}_p)\frac{\xi}{\eta} - p_{tiral}^n + K\Delta\boldsymbol{\varepsilon}_p^v = 0 \tag{30}$$

with

$$\dot{\boldsymbol{\varepsilon}}_p = \frac{\xi}{\eta}(\dot{\boldsymbol{\varepsilon}}_p^v) \tag{31}$$

By introducing the Eq. (31) into Eq. (30), the return-mapping equation for the apex of Drucker-Prager is as follows [4]:

$$r(\Delta\boldsymbol{\varepsilon}_p^v) \equiv c(\boldsymbol{\varepsilon}_p^{n-1} + \alpha\Delta\boldsymbol{\varepsilon}_p^v)\beta - p_{tiral}^n + K\Delta\boldsymbol{\varepsilon}_p^v = 0 \tag{32}$$

where

$$\alpha \equiv \frac{\xi}{\eta}, \quad \beta \equiv \frac{\xi}{\eta} \tag{33}$$

After computing the return-mapping in Eq. (32), the strain and stress can be updated by the following equations [4]:

$$\boldsymbol{\varepsilon}_p^n = \boldsymbol{\varepsilon}_p^{n-1} + \alpha\Delta\boldsymbol{\varepsilon}_p^v$$
$$\boldsymbol{\sigma^n} = -\left(\boldsymbol{p_{tiral}^n} - \boldsymbol{K\Delta\varepsilon_p^v}\right)\boldsymbol{I} \tag{34}$$

After solving the Eq. (34), the stress and strain are updated.

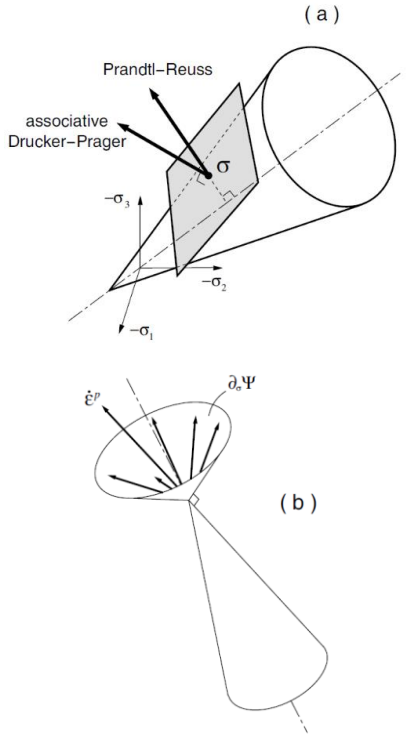

Fig. 2 . The Drucker–Prager flow vector; (a) cone surface, and (b) apex [4].

4. NUMERICAL RESULTS

To validate Darker-Prager elastoplastic model and the numerical integration algorithm stated for this model in this study, the numerical results obtained from this algorithm should be compared and evaluated with analytical, laboratory or other software results. Therefore, in this study, numerical results are compared with laboratory results and the results of numerical modeling with Abaqus software, and the validation of the developed algorithm is described below.

4. 1. Triaxial Test Results

To validate the numerical integration developed in this study, the triaxial test results conducted by Zhang [31] are used. In his study,

triaxial compression tests were carried out on the claystone samples to measure mechanical parameters. The procedure was done, as follows: I) Hydrostatic compaction up to 15 MPa was applied to the sample, II) Deviatoric loading was performed under displacement control which corresponds to an axial compression strain rate of $1 * 10^{-6}\ s^{-1}$.

To check the validation of the numerical integration algorithm developed in this study, the strain and stress results obtained from triaxial test are chosen. Then the strain values, including axial strain and radial strain, are entered into the developed integration algorithm.

The numerical results of the integration algorithm developed in this study are compared with the triaxial test results. The results of this comparison, which are shown in Fig. 3 and Fig. 4, include the investigation of two different behaviors of stress and strain, which are a) Axial and radial stress difference $(\sigma_a - \sigma_r)$ versus axial strain ε_a and b) Axial and radial stress difference $(\sigma_a - \sigma_r)$ versus radial strain ε_r.

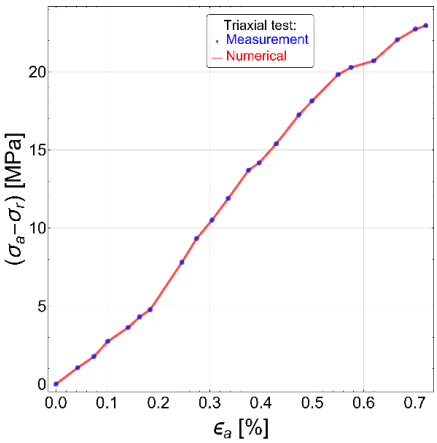

Fig. 3. Comparing the results of $(\sigma_a - \sigma_r)$ versus ε_a obtained from the integration algorithm developed in this study with the triaxial test results.

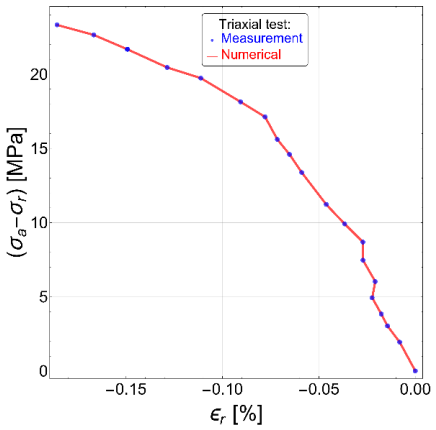

Fig. 4. Comparing the results of $(\sigma_a - \sigma_r)$ versus ε_r obtained from the integration algorithm developed in this study with the triaxial test results.

The results indicated in Fig. 3 and Fig. 4 illustrate that the numerical results computed from the numerical integration algorithm presented in this study are in good agreement with the triaxial test results.

4. 2. Numerical Modeling Of Triaxial Test

To validate the integration algorithm, the numerical modeling of the triaxial compression test on the rock sample was performed in Abaqus software. In this modeling, the diameter of the rock sample is 70 mm and its length is 140 mm. The sample is loaded similar to the triaxial test to obtain the stress-strain behavior of the rock.

The input parameters for numerical modeling are reported in Table 1. Numerical modeling of triaxial test was done in two dimensions. The model has a rectangular geometry similar to Fig. 5, and it is actually a quarter of the original sample, that is, the width of the model is 35 mm and its length is 70 mm. The selected constitutive model for elastoplastic behavior in Abaqus software is Drucker-Prager model. The conditions of numerical modeling are similar to the real test. In this model, first the sample is subjected to hydrostatic loading by applying a constant confined stress of 15 MPa on the right side and top of the sample in the x (horizontal) and y (vertical) directions, respectively. Then, the upper boundary of the sample is loaded at a rate of -0.0005 m/s. In this modeling, the normal displacement in the left and bottom boundaries of the model is assumed to be zero. The duration of the test is 30 seconds.

Table 1. Input parameters for numerical modeling

Parameter	Value
Density of rock, ρ [kg/m^3]	2700
Young's modulus, E [GPa]	45
Poisson's ratio, υ	0.32
Flow stress ratio, f	1
Friction angle, φ [°]	24

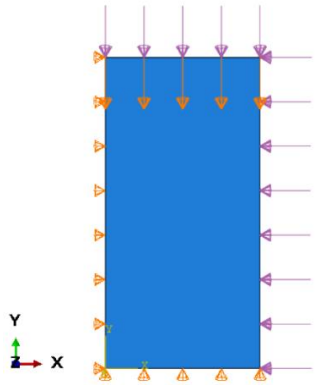

Fig. 5. Geometry of the numerical model and its boundary conditions.

The numerical results of the displacement from the triaxial test performed in Abaqus software, are shown in Fig. 6.

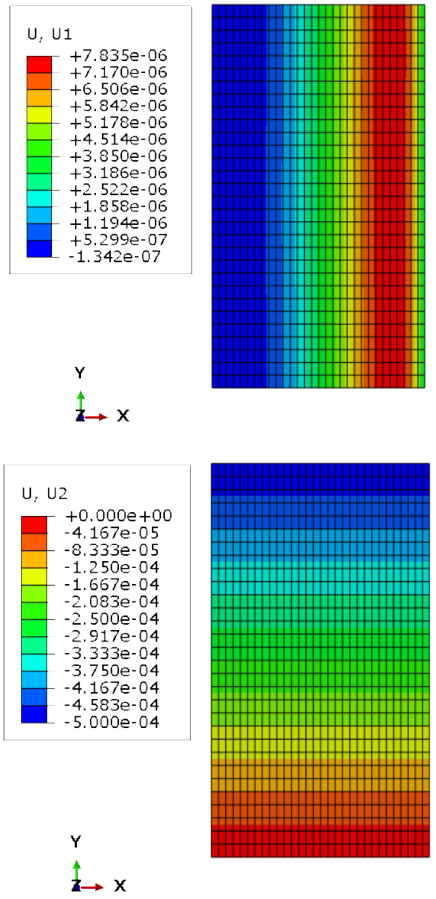

Fig. 6. Displacement counter: (top) U1, (bottom) U2.

To check the validation of the numerical integration algorithm developed in this study, the strain and stress results obtained from an element of the model in Abaqus, as shown in Fig. 7 with the black circle, are selected. Then the parameters of Table 1 and strain values, including axial strain and radial strain, are entered into the developed integration algorithm.

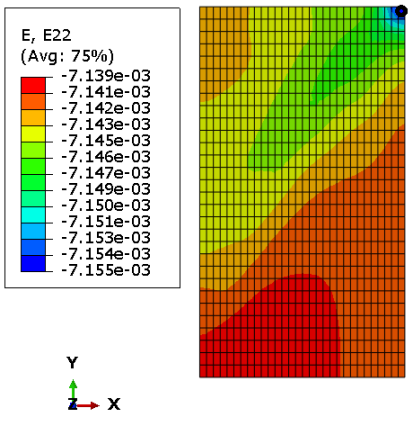

Fig. 7. Strain E22 and selected element with black circle.

The numerical results of the integration algorithm developed in this study are compared with the numerical modeling results of Abaqus. The results of this comparison, which are illustrated in Fig. 8 and Fig. 9, include the investigation of two different behaviors of stress and strain, which are a) Axial and radial stress difference $(\sigma_a - \sigma_r)$ versus axial strain ε_a and b) Axial and radial stress difference $(\sigma_a - \sigma_r)$ versus radial strain ε_r.

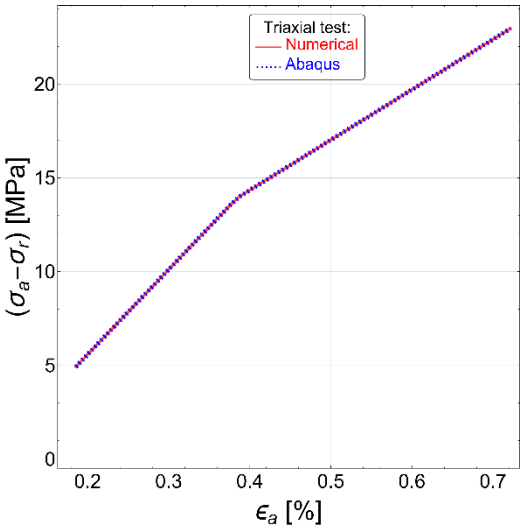

Fig. 8. Comparing the results of $(\sigma_a - \sigma_r)$ versus ε_a obtained from the integration algorithm developed in this research with the results of Abaqus software.

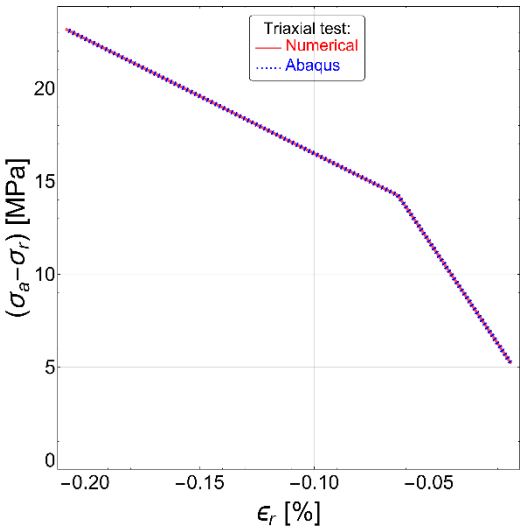

Fig. 9. Comparing the results of $(\sigma_a - \sigma_r)$ versus ε_r obtained from the integration algorithm developed in this research with the results of Abaqus software.

The results shown in Fig. 8 and Fig. 9 indicate that the numerical results obtained from the numerical integration algorithm developed in this research are in good agreement with the results obtained from Abaqus software. The good conformity of the results, in addition to confirming the correctness of the presented algorithm, makes

it possible for the author of the article to use this algorithm in home-made programming code to express the elastoplastic behavior in his geomechanical studies in the future in order to increase the accuracy of modeling. In addition, the Drucker-Prager criterion implemented in this research may be used by users for intact rock or rock mass. Basically, its use and its correlation with the results obtained from the experimental test depends on the anisotropy of the data.

5. CONCLUSIONS

The description provided for the Darker-Prager criterion and the fundamental integration algorithm developed in this study provides this possibility for the interested readers to implement the Darker-Prager elastoplastic model. The model developed in this research has the following results:

- The proposed integration algorithm consists of only two elastic trial step and plastic return-mapping algorithm, which makes its coding and implementation easier.
- The advantage of developed algorithm is its numerical stability, which will generally lead to fast convergence and stable algorithm.
- The developed integration algorithm can be used as a suitable infrastructure to provide elastoplastic models in home-made developed software codes or software under development.

REFERENCES

[1] Rezaiee-Pajand, M., Sharifian, M. and Sharifian, M. (2011). Accurate and approximate integrations of Drucker–Prager plasticity with linear isotropic and kinematic hardening. European Journal of Mechanics - A/Solids, Volume 30(3): 345-361. https://doi.org/10.1016/j.euromechsol.2010.12.001.

[2] Borja, Ronaldo I. (2013). Plasticity. Springer Berlin Heidelberg. doi: 10.1007/978-3- 642-38547-6 (cit. on pp. 91, 92).

[3] Rezaiee-Pajand, M. and Nasirai, C. (2008). On the integration schemes for Drucker-Prager's elastoplastic models based on exponential maps. Int. J. Numer. Meth. Eng. 74: 799-826.

[4] de Souza Neto E, Peri D, and Owen D. (2008). Computational methods for plasticity. John Wiley Sons Ltd.

[5] Loret, B. and Prevost, J.H. (1986). Accurate numerical solutions for Drucker–Prager elastic–plastic models Comput. Meth. Appl. Mech. Eng.

[6] Genna, F. and Pandolfi, A. (1994). Accurate numerical integration of Drucker-Prager's constitutive equations. Meccanica 29: 239-260.

[7] Kobayashi, M., Mukai, M., Takahashi, H., Ohno, N., Kawakami, T. and Ishikawa, T. (2003). Implicit integration and consistent tangent modulus of a time-dependent nonunified constitutive model. Int. J. Numer. Meth. Eng. 58: 1523-1543.

[8] Kan, Q.H., Kang, G.Z. and Zhang, J. (2007). A unified visco-plastic constitutive model for uniaxial time-dependent ratchetting and its finite element implementation. Theor. Appl. Fract. Mech. 47: 133-144.

[9] Coombs, W.M., Crouch, R.S. and Augarde, C.E. (2010). Reuleaux plasticity: analytical backward Euler stress integration and consistent tangent. Comput. Methods Appl. Mech. Eng. 199: 1733-1743.

[10] Liu, C.-S. (2004). Internal symmetry groups for the DruckerePrager material model of plasticity and numerical integrating methods. Int. J. Solids Struct. 41: 3771-3791.

[11] Cecílio D.L., Devloo P.R., Gomes S.M., dos Santos E.R. and Shauer N. (2015). An improved numerical integration algorithm for elastoplastic constitutive equations. Comput Geotech, 64: 1–9.

[12] Sanei, M., Devloo, P.R.B., Forti, T.L.D., Durán, O. and Santos, E.S.R. (2021a). An innovative scheme to make an initial guess for iterative optimization methods to calibrate material parameters of strain-hardening elastoplastic models. Rock Mech Rock Eng 55(1): 399–421. https:// doi. org/ 10. 1007/ s00603- 021- 02665-y.

[13] Sanei, M., Devloo, P.R.B., Forti, T.L.D., Durán, O. and Santos, E.S.R. (2019). On data adjustment of an elastoplastic constitutive model using optimization methods. ENAHPE 2019 – Encontro Nacional de Construção de Poços de Petróleo e Gás Serra Negra – SP, 19 a 22 de Agosto de 2019.

[14] Sanei, M., Durán, O., Devloo, P.R.B. and Santos, E.S.R. (2021b). Analysis of pore collapse and shear-enhanced compaction in hydrocarbon reservoirs using coupled poro-elastoplasticity and permeability. Arab J Geosci. https:// doi. org/ 10. 1007/ s12517- 021-06754-8.

[15] Sanei, M., Durán, O., Devloo, P.R.B., Santos, E.S.R. (2022). Evaluation of the impact of strain-dependent permeability on reservoir productivity using iterative coupled reservoir geomechanical modeling. Geomech Geophy Geo Energy Geo Res. https:// doi. org/ 10. 1007/ s40948- 022- 00344-y.

[16] Sanei, M., Duran, O., Devloo, P.R.B. (2019). Numerical modeling of pore collapse in hydrocarbon reservoirs using a cap plasticity constitutive model. In Proceedings of the 14th International Congress on Rock Mechanics and Rock Engineering, Brazil. ISRM-14CONGRESS-2019-377.

[17] Durán, O., Sanei, M., Devloo, P.R.B., Santos, E.S.R. (2019). An iterative scheme for poroelasto-plastic to analyze a wellbore during drilling. ENAHPE 2019 –

Encontro Nacional de Construção de Poços de Petróleo e Gás Serra Negra – SP, 19 a 22 de Agosto de 2019.

[18] Sanei, M., Duran, O., Devloo, P.R.B. (2017). Finite element modeling of a nonlinear poromechanic deformation in porous media. In Proceedings of the XXXVIII Iberian Latin American Congress on Computational Methods in Engineering. ABMEC Brazilian Association of Computational Methods in Engineering. https:// doi. org/ 10. 20906/ cps/ cilamce 2017- 0418.

[19] Duran, O., Sanei, M., Devloo, P.R.B., Santos, E.S.R. (2020). An enhanced sequential fully implicit scheme for reservoir geomechanics. Comput Geosci 24(4): 1557–1587. https:// doi. org/ 10. 1007/ s10596- 020- 09965-2.

[20] Sanei, M., Duran, O., Devloo, P.R.B., Santos, E.S.R. (2020). An innovative procedure to improve integration algorithm for modified cam-clay plasticity model. Comput Geotech 124: 103604. https://doi.org/10.1016/j.compgeo.2020.103604.

[21] Heydari, M., Aghakhani Emamqeysi, M.R., Sanei, M. (2022) Finite element analysis of wellbore stability and optimum drilling direction and applying NYZA method for a safe mud weight window. Journal of Analytical and Numerical Methods in Mining Engineering. 10.22034/ANM.2022.2582.

[22] Rudnicki, John W. (1986). Fluid mass sources and point forces in linear elastic diffusive solids. In: Mechanics of Materials 5(4): 383–393. doi: 10.1016/0167- 6636(86)90042-6.

[23] Kossa, A. (2011). Exact stress integration schemes for elastoplasticity Ph.D. thesis Budapest University of Technology and Economics.

[24] Davis, R and Selvadurai, A. (2002). Plasticity and geomechanics. Cambridge University Press.

[25] Sanei, M., Faramarzi, L., Fahimifar, A., Goli, S., Mehinrad, A., Rahmati, A. (2015). Shear strength of discontinuities in sedimentary rock masses based on direct shear tests. Int. J. Rock Mech. Min. Sci., 75:119-131. https://doi.org/10.1016/j.jksus.2023.102846.

[26] Sanei, M. (2023). Development of Mohr-Coulomb criterion elastoplastic integration algorithm scheme for rock. Journal of Petroleum Geomechanics. 10.22107/JPG.2023.413537.1209.

[27] Drucker, D.C. and Prager, W. (1952). Soil Mechanics and Plasticity Analysis of Limit Design. Quart. J. Appl. Math., 10: 157–162.

[28] Chen, W-F. and Mizuno, E. (1990). Nonlinear Analysis in Soil Mechanics. Theory and Implementation. New York: Elsevier.

[29] H Yousefian, H Soltanian, MF Marji, A Abdollahipour, Y Pourmazaheri. (2018). Numerical simulation of a wellbore stability in an Iranian oilfield utilizing core data. Journal of Petroleum Science and Engineering 168, 577-592.

[30] A Abdollahipour, MF Marji. (2020). A thermo-hydromechanical displacement discontinuity method to model fractures in high-pressure, high-temperature environments. Renewable Energy 153, 1488-1503.

[31] Zhang, C.L. (2016). The stress–strain–permeability behaviour of clay rock during damage and recompaction. In: Journal of Rock Mechanics and Geotechnical Engineering 8(1): 16–26.